Analyst

Accepted Manuscript

ROYAL SOCIETY OF CHEMISTRY

www.rsc.org/analyst

Screening and mapping pigments in paintings using scanning electrochemical microscopy (SECM)

Antonio Doménech-Carbó*[a], María Teresa Doménech-Carbó[b], Miguel Silva[b], Francisco Manuel Valle-Algarra[a], José Vicente Gimeno-Adelantado[a], Francisco Bosch-Reig[a], Rufino Mateo-Castro[a]

[a] Departament de Química Analítica. Universitat de València. Dr. Moliner, 50, 46100 Burjassot (València) Spain.
[b] Institut de Restauració del Patrimoni, Universitat Politècnica de València, Camí de Vera 14, 46022, València.

* Corresponding author. E-mail: antonio.domenech@uv.es.

Abstract

The use of the scanning electrochemical microscopy (SECM) technique for identifying and mapping both organic and inorganic pigments in sub-microsamples from pictorial specimens is described. This methodology, inspired in the voltammetry of immobilized particles technique, permits the study of textural properties of paint layers and mapping the distribution of pigment grains upon application of different potentials to the substrate. Combination of redox competition SECM strategy with voltammetric records yields local identification of different organic and inorganic pigments in paint samples.

Keywords: Scanning electrochemical microscopy; Atomic force microscopy-voltammetry of microparticles, Pigments; Mapping; Screening, nanoelectrochemistry

1. Introduction

The identification of the components of the different paint layers in works of art and decorative objects is of obvious importance for archaeometry, conservation and restoration. In particular, pigment screening can provide information on the provenance, pictorial technique and authenticity of the pieces. This analytical target is often made difficult by the high dilution of the pigments in the paint layers, its distribution in different strata and the presence of bindings, varnishes and other products, among them, those resulting from the chemical and/or biological deterioration of the painting and the need of using a minimal amount of sample as possible for performing the analyses.[1]

The determination of the chemical and mineralogical composition of the pigments in paintings can be achieved by means of a wide variety of analytical techniques, each one of them providing partial information, whose synergistic combination could satisfy the analytical demands.[2] Scanning electron microscopy with energy dispersive X-ray analysis (SEM/EDX) is typically used for studying the composition and local distribution of pigments in cross sections of paint layers. Although highly sensitive for inorganic pigments, this technique, however, becomes less sensitive for organic pigments mainly composed of C, O, H and N and, therefore, hardly detectable with conventional X-ray detection systems coupled to SEM.[3]

In this context, the voltammetry of immobilized particles (VIMP), a solid-state electrochemical methodology developed by Scholz et al.[4-10] prompting the electrochemical characterization of solid materials, was of interest because of its inherently high sensitivity and the use of few nanograms of sample, if required.[11,12] This methodology, whose immediate antecedent is the analysis of solids at carbon paste electrodes,[13-19] is based on the abrasive transference of several particles of the solid sample to the surface of an inert electrode in contact with a suitable electrolyte. The VIMP technique has been applied to the identification of inorganic pigments,[20-24] their alteration products,[22,25] metals[25] and metal corrosion products.[26-30] Additionally, as recently reviewed,[31] the VIMP can also provide relevant information for authentication,[32] technical grouping[33,34] and dating.[11,31,35-37]

Although graphite pencil sampling[38-41] and in situ cells[42-44] provided opportunity for local analysis, including layer-by-layer[45] and mapping,[46] there is a limitation in the spatial resolution acquired by means of such techniques. In order to expand the capabilities of solid-state electrochemical methodologies, scanning electrochemical microscopy (SECM) has been adapted to analyze microparticulate deposits of pigments and paint layers in a similar way to VIMP. SECM is an electrochemical technique, developed by Bard and Mirkin,[47] that provides information on electrochemical surface topography at the micrometer- sub-micrometer domain. SECM has been recently used in bioanalytical applications such as latent fingerprint detection,[48] imaging of morphological changes in single cells,[49] DNA hybridization[50] and genomic DNA microarrays,[51] but this technique has also been used for monitoring changes on coated metals immersed in aqueous electrolytes[52,53] and for evaluating the electrochemical activity of anti-corrosion coatings.[54]

Here, mapping of the pigment distribution into stratified paint layers is be achieved by using of a redox competition based strategy,[54-56] also prompting the discrimination between different types of pigments by applying different potential inputs to the sample. Combination of such strategy with the record of the voltammetric response of the electrolyte solution in the immediate vicinity of the paint layers permits the direct screening of pigments and, in particular, the identification of organic pigments. Complementary SEM/EDX and atomic force microscopy (AFM) experiments were performed following previously described approaches.[23]

2. Experimental

2.1. Instrumentation

Electrochemical experiments were performed at 298 K in a three-electrode cell under argon atmosphere using a CH I920c device (Cambria Scientific, Llwynhendy, Llanelli UK). A platinum wire counterelectrode and an AgCl (3 M NaCl)/Ag reference electrode completed the three-electrode arrangement. SECM experiments were performed with CH 920c equipment using a microdisk platinum electrode tip (CH 49, diameter 20 μm) and a Pt substrate electrode (geometrical area 0.018 cm^2). The bipotentiostat mode was used to

apply potentials to the tip (E_T) and the electrode substrate (E_S). The rate of scanning of the tip over the substrate was 20 μm/s for all experiments, the distance between tip and substrate being of the order of the tip electrode radius. All measurements were performed at room temperature (298±1 K) in solutions previously deaerated by bubbling argon during 15 min.

2.2. Materials and procedures

Aqueous 0.25 M sodium acetate buffer (Panreac) at pH 4.75 was used as the electrolyte for both VIMP and SECM experiments. The electrolyte was degasified by bubbling Ar during 10 min for VIMP experiments. Square wave voltammograms (SWVs), and cyclic voltammograms (CVs) were obtained using conventional abrasive VIMP protocols.[8] For SECM experiments, non-degasified solutions were employed in order to use dissolved oxygen as a redox probe, optionally accompanied by 2.0 mM $K_4Fe(CN)_6$. Commercial graphite leads (Staedtler HB, 68% wt graphite) were used for such experiments.

Paint specimens for SECM experiments were prepared by excising with a microscalpel a paint sample of ca. (0.5 × 0.5 × 0.5) mm sized and embedding it embedding in Glasspol® polyester polymer forming cubical blocks (4.0 × 4.0 × 4.0) mm sized. After hardening, the blocks were polished for both sides with abrasive CSi disks until a thin section of the sample ca. 0.5 mm sized was obtained. The thin sections were fixed to the substrate electrode by applying a ring of acetone solution of acrylic resin Paraloid B72® that surrounded the sample so that the paint sample was exposed by both the upper, lower and one lateral faces of the block as schematized in Figure 1. This arrangement enables application of potential inputs through the substrate electrode in contact with the sample whereas the upper region of the sample is close to the tip electrode.

Two types of thin-sections were prepared depending on the study to carry out: a) transversal thin-section that enabled the study of the different paint layers present in the painting from the ground to the varnish (see Figs. 1a,b) parallel thin-section that enabled the study of the outer/inner paint layers that conform the painting. Parallel and transversal arrangements of the paint samples were alternatively used for studying the different areas

of the painting. Complementary experiments were carried out on deposits of selected pigments on Pt substrate electrode fixed with the help of a porous fine coating of Paraloid B72® acrylic polymer as previously described for VIMP experiments.[20]

SECM experiments were performed by placing the above blocks onto the surface of a base electrode (Pt or a graphite bar) into the SECM cell and covering it with the electrolyte solution. The position of the blocks, depicted in Figure 1, was adjusted to ensure that one portion of the paint sample was in contact with the base electrode.

In situ AFM-monitored electrochemical experiments were performed with a multimode AFM (Digital Instruments VEECO Methodology Group, USA) with a NanoScope IIIa controller and equipped with a J-type scanner (max. scan size of 150×150×6 μm). The topography of the samples was studied in contact mode. An oxide-sharpened silicon nitride probe Olympus (VEECO Methodology Group, model NP-S) has been used with a V-shaped cantilever configuration. Transference of sample particles to a carbon plate and experimental conditions were similar to those previously described.[23]

2.3. Reference materials and paint samples

Pigments Naples yellow K43100, lead white (K46002), Spanish ochre (K11585) and hematite (K48651) were supplied by *Kremer pigmente* (Germany). Morin and alizarin were supplied by (Sigma-Aldrich). Copper(II) acetate and lead nitrate (Merck) were used for blank experiments.

Samples (ca. 0.5 mm sized) listed below were mechanically excised from "*Los Jurados de Valencia ante la Inmaculada*" (1662) by Jerónimo Jacinto de Espinosa using a microscalpel. Pigments identified by SEM-EDX from the outer to inner layer:

Sample S1: red-orange sample: paint layer 1, red earth; paint layer 2, white lead; ground, raw Sienna.

Sample S2: white sample. From the outer to inner: paint layer 1 white lead; ground: raw Sienna.

Sample S3: flesh sample. From the outer to inner: paint layer 1 azurite and madder grains dispersed in white lead layer; ground: raw Sienna.

3. Results and discussion

3.1. Pigment deposits

To explore the SECM response of the inorganic pigments, imaging of microparticulate deposits of different compounds on the surface of a Pt substrate electrode, was performed using generation/collection mode using dissolved oxygen[57] and $Fe(CN)_6^{4-}$ as redox probes. The hexacyanoferrate(II) oxidation leads to enhanced/decreased tip current (referred to as SECM positive/negative feedback) which enables us to study the electrode reactions that occur in the solution gap formed between the tip and the microparticulate substrate. Under our experimental conditions, the grains of pigment can be electrochemically oxidized/reduced upon application of a given potential to the substrate (E_S). Entirely equivalent results were obtained in air-saturated acetate buffer solutions in the absence of hexacyanoferrate upon applying to the tip a potential negative enough to promote the electrochemical reduction of dissolved oxygen, a well-known electrochemical process occurring at potentials of ca. –0.40 V in acetate buffer.[58,59]

Figure 2 shows SECM topographic images of two microparticulate deposits, (respectively, images 2a,b and 2c,d) of Naples yellow ($PbSbO_3$) on Pt substrate immersed into a 2.0 mM $K_4Fe(CN)_6$ plus 0.25 M HAc/NaAc solution at pH 4.75. SECM images were recorded by fixing the tip potential (E_T) at a value where $Fe(CN)_6^{4-}$ oxidation takes place under diffusion-controlled conditions, as ensured by voltammograms previously performed in the solution. When no potential was applied to the substrate (Fig. 2a,c), the exposed regions of the base electrode display a positive feedback response whereas the regions covered by the pigment grains produce negative feedback, consistently with the insulating nature of the tested compounds.

Figure 3 depicts the corresponding probe approach curves in terms of the ratio between the tip current at a distance d and the tip current at infinite distance, I/I_∞ vs. the d/r ratio (r = tip radius). The I/I_∞ ratio initially rises on approaching the sample, but then reaches a maximum and falls sharply. This response, which differs from those expected for a

purely negative feedback (expected on approaching over the pigment grains) and a purely positive feedback (expected on approaching to the bare electrode) on flat insulating surfaces, can in principle be attributed to the partially hindered diffusional transport of the $Fe(CN)_6^{4-}$ probe resulting from the irregular nature of the particulate deposit which consists, as indicated by AFM examination (see below) of aggregates of grains 2-6 μm sized defining a rough surface.

When no potential was applied to the substrate (Fig. 2a,c), SECM topographic images showed negative feedback irregular regions surrounded by the 'flat' base electrode contour of positive feedback. For our purposes, the relevant point to emphasize is that applications of potential inputs to the pigment grains should produce topographic changes associated to the change in the composition of the pigment. Thus, in acetate buffer, as previously described,[20,23] Naples yellow is electrochemically reduced at a potential of ca. −0.65 V to Pb metal, a process which can be represented by the equation:

$$Pb_3(SbO_4)_2\ (solid) + 4H_2O + 4H^+\ (aq) + 6e^- \rightarrow 3Pb\ (solid) + 2Sb(OH)_6^-\ (aq) \quad (1)$$

When a potential less negative than −0.45 V is applied to the substrate, the SECM image remains essentially unchanged, as can be seen on comparing Figs. 2a and 2b. This means that, under our experimental conditions, such potential inputs do not produce changes in the microparticulate deposit of Naples yellow altering significantly the topography as given by the tip-sample surface local distance. It is pertinent to note, however, that such changes can only be determined as far as the separation and amplitude of the sample surface modifications

On the contrary, when the substrate potential is held at a value negative enough to promote the reduction of the pigment, significant topographic changes were observed. As it can be seen on comparing Figs. 2c and 2d, in several regions there is an engrossment of several regions of negative feedback (marked by continuous arrows in Fig. 2d) while in contiguous regions the contrary effect was observed (marked by dotted arrows). These features can be rationalized on the basis of AFM studies from Hasse and Scholz of the reduction different lead and silver compounds.[60-62] The electrochemical reduction of metal compounds to the corresponding metal can involve a topotactic

reduction process via formation of an intermediate hydrated layer resulting in the formation of an amorphous metal layer, followed by recrystallization. Accordingly, the original crystal of the metal compound is progressively converted into metal which form an adjacent crystal determining the apparent engrossment of the negative feedback region. Consistently with this scheme, SECM images in Fig. 2 show changes in the crystal/electrolyte/substrate electrode junction which can be described in terms of the progressive conversion of the crystal aggregates of Naples yellow into adjacent deposits of Pb metal (see also Supporting information, Figure S3). Under these experimental conditions, some lead pass to the solution phase as Pb^{2+} (aq), as denoted by the appearance of typical stripping peaks for Pb in the voltammograms recorded using the tip as a working electrode (*vide infra*).

In several other cases, the involved electrochemical process consists of the reductive dissolution of the compound. This is the case of earth pigments,[21,63-65] typically represented by the reduction of goethite mineral as:

$$FeO(OH)\ (solid) + 3H^+\ (aq) + e^-\ \rightarrow\ Fe^{2+}\ (aq) + 2H_2O \qquad (2)$$

Figure 4 shows the topographic SECM images of a deposit of Spanish ochre on Pt substrate immersed into $K_4Fe(CN)_6$ solution in acetate buffer when there is no applied potential to the substrate (Fig. 4a) and applying a substrate potential sufficiently negative to promote the reductive dissolution of Fe(III) minerals[21,63-65] (Fig. 4b). Here, it was observed the progressive decrease of the negative feedback features in the regions which could correspond to the lateral faces of the pigment grains. The height decreased significantly while the roughness increased as indicated in Table S.1 (Supplementary information). This observation can be attributed to the reductive dissolution of the crystals under diffusion-limited conditions when the surroundings of crystals are saturated by Fe^{2+} ions, as theoretically described by Grygar.[63] The same features were observed upon AFM imaging of deposits of iron pigments on highly oriented pyrolytic graphite plate (HOPG) in contact with aqueous acetate buffer. See Figure 5 for hematite.

In the case of organic pigments in contact with aqueous electrolytes, there is possibility of proton-assisted topotactic solid-to-solid transformations accompanied by processes

where a soluble compound is formed. In most anthraquinonic and flavonoid dyes, this electrochemistry is based on quinone/catechol redox interconversions.[66-70] Such processes involve obvious modifications in the molecular structure but also significant changes in the intermolecular hydrogen bonding system, which plays an important role in the cohesion of the solids. Accordingly, the application of oxidative or reductive potential inputs results in significant morphological modifications of dye crystals. This can be seen in Fig. 6, where the AFM images of a deposit of morin crystals attached to a HOPG plate in contact with aqueous acetate buffer, are depicted before and after application of an oxidative potential step. Here, the oxidation process is accompanied by the progressive corrugation of the crystals with dissolution and subsequent precipitation of minor irregular crystals of an oxidized compound. At the scale of SECM experiments, this kind of processes should produce changes in the topographic features (*vide infra*).

3.2. Paint samples

Local analysis of paint samples was performed by SEM/EDX before SECM experiments. This analysis permitted the detection of iron, lead, copper, etc. pigments but is not conclusive on the presence of organic pigments.[3] Thin-sections of paint samples prepared as described previously and placed onto the Pt substrate were also analyzed by SCEM. As a result, the inner/outer surface of the sample or the transversal section containing the different paint layers was exposed, optionally, so that pigment mapping in one or several layers could be made. Reported data are concentrated in cross-sections (scheme in Fig. 1a) for their major interest for conservation and restoration purposes. An example of parallel sampling (Fig. 1b) is provided as a Supplementary material (Fig. S6). Figure 7a depicts the SECM image of a cross-section of paint sample S1, taken from the painting "*Los Jurados de Valencia ante la Inmaculada*", where the tip current variations can be clearly associated to three different paint strata. Figure 7b shows the microphotograph (PPL) obtained with a light microscopy where three pictorial strata can be discerned.

Sequential application of different potentials to the substrate, using the redox competition philosophy,[54-56] can yield information on the composition and distribution of pigment particles. Figure 8 shows the SECM topographic images of paint sample S2

(photomicrograph of the transversal thin-section is provided as supplementary electronic material, Fig S.1, indicating the SECM scanned area) arranged transversally on Pt substrate immersed into 2.0 mM $K_4Fe(CN)_6$ plus 0.25 M HAc/NaAc when a potential of +0.30 V is applied to the tip and the substrate electrode is held at a) 0.00, b) −0.45, and c) −0.70 V. The first image permits to distinguish the embedding polymer and the first pictorial layer with rounded negative feedback features. Upon application of a potential of −0.45 V to the substrate, some of such features vanished, thus suggesting that earth pigments experiencing reductive dissolution processes existed. Subsequent imaging upon applying a potential of −0.70 V to the substrate, able to reduce lead pigments (and maintaining the reductive dissolution of earths) resulted in the expansion and height increase of several spots, then attributable to the deposition of lead, thus confirming the presence of lead white in the paint layer, as suggested by the white color (Fig. S.1) and SEM/EDX data. When applied this strategy to the subsequent paint layers, only topographic changes associated to reductive dissolution of earths were observed, thus denoting that the lead pigment was used exclusively in the more external layer.

Figure 9 compares the topographic profile of another region of the first layer of sample S2 upon applying potentials of 0.00 and −0.70 V to the substrate. In the first image, one can distinguish a peaked feature corresponding to a lead white grain near to the surface of the paint layer in the vicinity of the flat region of the embedding polymer. Applying a potential sufficiently negative to produce the reduction of the pigment, the peaked topography of the grain became modified with formation of an adjacent deposit of Pb metal, now appearing as a second negative feedback feature.

In order to illustrate the capability of the proposed methodology for screening organic pigments, a third flesh sample S3 (photomicrograph of the transversal thin-section is provided as supplementary electronic material, Fig S.2), which contained grains of madder (organic pigment extracted from the plant *Rubia tinctorum* containing alizarin and purpurin as coloring compounds) and azurite dispersed in a white layer made with lead white was tested. Figure 10 depicts the SECM topographic images of a sample from sample S3 arranged transversally on Pt substrate immersed into air-saturated 0.25 M HAc/NaAc, pH 4.75. To identify the presence of the different pigments, a series of

voltammograms were recorded before and after each one of the above scanning experiments using the tip as a working electrode. The tip was maintained in its original position before each series of SECM scans; i.e., immersed in the electrolyte solution in the vicinity of the paint sample at a distance of 20 μm of the average level of each paint specimen. In these conditions, the voltammogram should reflect the local composition of the solution in this region so that the electrochemical response of species released from the paint sample as a result of the application of reductive or oxidative potential inputs could be recorded. Blank experiments were performed in solutions of copper(II) acetate, lead(II) nitrate and alizarin in acetate buffer, using the Pt tip as a working electrode.

Successive scanning experiments were performed upon applying a tip potential negative enough to promote the reduction of dissolved O_2 (–0.45 V) and applying different potentials to the substrate. When no potential was applied to the substrate (Fig. 10a), the image shows the paint layer with diffuse contour with several negative feedback features, attributable to different pigment grains. When a potential of +0.40 V was applied to the substrate (Fig. 10b), local engrossments of negative feedback features appeared. At this potential, several anthraquinonic and flavonoid pigments are oxidized[66-70] so that the topographic changes can be associated to the regions where grains of such pigments are located within the paint layer. As far as the pigment grains are surrounded by the pictorial binder, the engrossment of the negative feedback features could be due to: i) the alteration of altering the density and texture of the embedding binding components permeated by the oxidized compounds, possibly increasing in volume; ii) the creation of additional constraints to the diffusion of dissolved O_2 to the tip electrode when such organic species diffuse into the surrounding electrolyte.

Figure 11a shows the SWV recorded at the tip working electrode just after the SECM experiment in Fig. 10b. To avoid the interference of proton discharge at Pt electrode, only potentials less negative than –0.45 V were applied in the recorded voltammograms. Here, an anodic wave appears at +0.45 V, corresponding to the electrochemical oxidation of alizarin (blank experiments at alizarin solution) released to the solution phase during the precedent SECM experiment. In a subsequent SECM experiment, the

substrate potential was held at –0.20 V. At this potential, azurite is reduced to Cu metal[20,28,41,46] so that the topography of the paint layer changes significantly (see Figure 10c). Now, the precedent alizarin feature vanishes while other local negative feedback features appear.

The subsequent voltammogram at the tip working electrode yields (see Fig. 11b) the signal for alizarin oxidation accompanied by two overlapping oxidation peaks corresponding to the stripping of Cu at ca. 0.0 V, coincident with blank experiments in Cu(II) solutions in acetate buffer. In agreement with extensive VIMP literature,[8-10] the appearance of these two signals can be attributed to the oxidation of different Cu deposits, a feature possibly associated to the different reductive processes experienced by azurite grains having different shape and size. The sequence of substrate potentials was completed by the application of a negative enough to promote the reduction of lead pigments.[20,23,35,36] The topographic profile (Fig. 10d) changes again relative to the precedent experiment showing several engrossed local negative feedback features, attributable to the deposition of lead metal in the vicinity of the lead white grains. The process, as in the case of azurite reduction, involves to some extent the release of metal ions to the solution phase. Accordingly, the subsequent voltammogram (Fig. 11c) in the electrolyte layer near the paint sample shows a prominent stripping signal for Pb at –0.40 V accompanied by a satellite signal at –0.48 V, again in agreement with blank experiments and literature data.[20,23,32,35,36] These features confirm the presence of lead white in the sample. Apart from the heterogeneity in the shape and size distribution of the pigment grains, the appearance of peak splitting in the stripping signals for Cu and Pb could be attributed to the involvement of Cu^{2+} (aq) and Pb^{2+} (aq) species and their reduction to a deposit of Cu and Pb metals differing from that resulting from the topotactic reduction of the pigment.[35,36,40,41,45]

4. Conclusions

Application of SECM to painting sub-microsamples from works of art inspired in the voltammetry of immobilized particles methodology permits the study of textural properties of paint layers and mapping the distribution of both organic and inorganic pigment grains. The proposed method of preparation of thin-sections of paint samples provides stable parallel and transversal arrangements suitable for the examination of

individual layers. Sequential application of different potentials to the substrate, based on redox competition strategies allows discriminating between different pigments on the basis of their different topographic features. These results illustrate the capabilities of nanoelectrochemical techniques for providing analytical information in the fields of archaeometry, conservation and restoration.

Acknowledgements: Research was conducted within the "*Grupo de análisis científico de bienes culturales y patrimoniales y estudios de ciencia de la conservación*" Microcluster of the University of Valencia Excellence Campus. Financial support is gratefully acknowledged from the MICIN Projects CTQ2011-28079-CO3-01 and 02 and CTQ2014-53736-C3-2-P which are also supported with ERDF funds. The authors would like to thank to Dr. José Luis Moya López and Mr. Manuel Planes Insausti (MS, UPV) technical supervisors responsible for the *Servicio de Microscopía Electrónica* de la Universitat Politècnica de València for their technical support.

References

1 T. J. Reedy and Ch.L. Reedy, *Statistical Analysis in Art Conservation Research*, The Getty Conservation Institute, Los Angeles, 1988.

2 F. Mairinger and M. Schreiner *New methods of chemical analysis-a tool for the conservator, Science and Technology in the service of conservation*, IIC, London, 1982, pp. 5-13.

3 P. Van Espen in A. G. Fitzgerald, B. E. Storey and D. Fabian (Eds) *Quantitative Microbeam Analysi*s, Institute of Physics Publishing, Bristol and Philadelphia, 1992, pp. 247-274.

4 F. Scholz, L. Nitschke and G. Henrion, *Naturwiss*., 1989, **76**, 71.

5 F. Scholz, L. Nitschke, G. Henrion and F. Damaschun, *Naturwiss*., 1989, **76**, 167.

6 F. Scholz, L. Nitschke and G. Henrion, *Fresenius Z. Anal. Chem*., 1989, **334**, 56.

7 F. Scholz, L. Nitschke, G. Henrion and F. Damaschun, *Fresenius Z. Anal. Chem*., 1989, **335**, 189.

8 F. Scholz and B. Meyer, *Electroanalytical Chemistry, A Series of Advances* vol. 1989, vol. 20, pp. 1-86.

9 F. Scholz, U. Schröder, R. Gulabowski and A. Doménech-Carbó, *Electrochemistry of Immobilized Particles and Droplets*, 2nd edit. Monographs in Electrochemistry Series, F. Scholz, Ed. Springer, Berlin-Heidelberg, 2014.

10 A. Doménech-Carbó, J. Labuda and F. Scholz, *Pure Appl. Chem*. (IUPAC Technical Report), 2013, **85**, 609.

11 A. Doménech-Carbó, M. T. Doménech-Carbó and V. Costa, Electrochemical Methods in Archaeometry, Conservation and Restoration. Monographs in Electrochemistry Series, F. Scholz, Ed. Springer, Berlin-Heidelberg, 2009.

12 A. Doménech-Carbó, *J. Solid State Electrochem*., 2010, **14**, 363.

13 R. N. Adams, *Anal. Chem.*, 1958, **30**, 1576.

14 T. Kuwana and W. G. French, *Anal. Chem*., 1964, **36**, 241.

15 D. Bauer and M. P. Gaillochet, *Electrochim. Acta*, 1974, **19**, 597.

16 Kh. Z. Brainina and R. P. Lesunova, *Zh. Anal. Khim*., 1974, **29**, 1302.

17 Kh. Z. Brainina and M. B. Vidrevich, *J. Electroanal. Chem*., 1981, **121**, 1.

18 V. I. Belyi, T. P. Smirnova and N. F. Zakharchuk, *Appl. Surf. Sci*., 1989, **39**, 161.

19 V. I. Belyi, T. P. Smirnova and N. F. Zakharchuk, *Thin Solid Films*, 1989, **113**, 157.

20 A. Doménech-Carbó, M. T. Doménech-Carbó, M. Moyá-Moreno, J. V. Gimeno-

Adelantado and F. Bosch-Reig, *Anal. Chim. Acta*, 2000, **407**, 275.

21 A. Doménech-Carbó, M. T. Doménech-Carbó, J. V. Gimeno-Adelantado, F. Bosch-Reig, M. C. Saurí-Peris and S. Sánchez-Ramos, *Analyst*, 2001, **126**, 1764.

22 A. Doménech-Carbó, M. T. Doménech-Carbó and H. G. M. Edwards, *Electroanalysis*, 2007, **19**, 1890.

23 A. Doménech-Carbó, M. T. Doménech-Carbó and X. Mas-Barberá, *Talanta*, 2007, **71**, 1569.

24 A. Doménech-Carbó, M. T. Doménech-Carbó and H. G. M. Edwards, *Anal Chem.,* 2008, **80**, 2704.

25 V. Costa, K. Leyssens, A. Adriaens, N. Richard and F. Scholz, *J. Solid State Electrochem*., 2010, **14**, 449.

26 N. Souissi, L. Bousselmi, S. Khosrof and E. Triki, *Mater. Corros*., 2004, **55**, 284.

27 M. Serghini-Idrissi, M. C. Bernard, F. Z., Harrif, S. Joiret, K. Rahmouni, A. Srhiri, H. Takenouti, V. Vivier and M. Ziani, *Electrochim. Acta*, 2005, **50**, 4699.

28 A. Doménech-Carbó, M. T. Doménech-Carbó and I. Martínez-Lázaro, *Microchim. Acta*, 2008, **162**, 351.

29 D. Satovic, S. Martinez and A. Bobrowski, *Talanta*, 2010, **81**, 1760.

30 F. Arjmand and A. Adriaens, *J. Solid State Electrochem*. 2012, **16**, 535.

31 A. Doménech-Carbó, *Anal. Methods*, 2011, **3**, 2181.

32 A. Doménech-Carbó, M. T. Doménech-Carbó, M. A. Peiró-Ronda and L. Osete-Cortina, *Archaeometry*, 2011, **53**, 1193.

33 A. Doménech-Carbó, M. T. Doménech-Carbó, M. L. Vázquez de Agredos-Pascual, *J. Phys. Chem. B*, 2006, **110**, 6027.

34 A. Doménech-Carbó, M. T. Doménech-Carbó, M. L. Vázquez de Agredos-Pascual, *Anal. Chem*., 2007, **79**, 2812.

35 A. Doménech-Carbó, M. T. Doménech-Carbó, M. A. Peiró-Ronda, Anal. Chem., 2011, **83**, 5639.

36 A. Doménech-Carbó, M. T. Doménech-Carbó, M. A. Peiró-Ronda, I. Martínez-Lázaro and J. Barrio, *J. Solid State Electrochem*., 2012, **16**, 2349.

37 A. Doménech-Carbó, M. T. Doménech-Carbó, S. Capelo, T. Pasíes and I. Martínez-Lázaro, *Angew. Chem. Int. Ed*., 2014, **53**, 9262.

38 D. Blum, W. Leyffer and R. Holze, *Electroanalysis*, 1996, **8**, 296.

39 V. Costa and F. Urban, *Reviews in Conservation*, International Institute of Conservation, 2005, vol. 6, p. 48.

40 A. Doménech-Carbó, M. T. Doménech-Carbó, M. A. Peiró-Ronda, *Electroanalysis*, 2011, **23**, 1391.

41 A. Doménech-Carbó, M. T. Doménech-Carbó T. Pasies and M. C. Bouzas, *Electroanalysis*, 2011, **23**, 2803.

42 P. Letardi, A. Beccaria, M. Marabelli and G. D'Ercoli, Development of electrochemical impedance spectroscopy as a tool for outdoors bronze corrosion characterization, in *2nd international congress on science and technology for the safeguard of cultural heritage in the Mediterranean basin, Paris*. Elsevier, Amsterdam, 2000, pp. 407-411.

43 F. Rodríguez, J. Genescá and J. Uruchurtu, *J. Appl. Electrochem*., 2010, **40**, 311.

44 Y. V. Roblinetskaya, E. O. Il'inykch and V. V. Slepushkin, *J. Anal. Chem*., 2011, **66**, 84.

45 A. Doménech-Carbó, M. Lastras, F. Rodríguez and L. Osete-Cortina, *Microchem. J*., 2013, **106**, 41.

46 A. Doménech-Carbó, M. T. Doménech-Carbó and I. Martínez-Lázaro, *Anal. Chim. Acta*, 2010, **610**, 1.

47 A. J. Bard and M. V. Mirkin, Eds. *Electrochemical Microscopy*, Taylor & Francis, Boca Raton, 2001.

48 M. Zhang and H.H. Girault, *Analyst*, 2009, **134**, 25.

49 W. Wang, Y. Xiong, F. –Y. Du, W. –H. Huang, W.- Z. Wu, Z. –L. Wang, J. –K. Cheng and Y. –F. Yang, *Analyst*, 2007, **132**, 515.

50 E. Fortin, P. Malley, L. Lacroix and S. Szunerits, *Analyst*, 2006, **131**, 186.

51 W.S. Roberts, F. Davis and S. P. J. Higson, *Analyst*, 2009, **134**, 1302.

52 A. C. Bastos, A. M. Simões, S. González-García, Y. González-García and R. M. Souto, *Progr. Org. Coat*., 2005, **53**, 177.

53 R. M Souto, Y. González-García, S. González, *Progr. Org. Coat*., 2009, **65**, 435.

54 D. A. Walsh, L. E. Li, M. S. Bakare and K. T. Voisey, *Electrochim. Acta*, 2009, **54**, 4647.

55 K. Karnicka, K. Eckhard, D. A. Guschin, L. Stoica, P. J. Kulesza and W. Schumann. *Electrochem. Commun*., 2007, **9**, 1998.

56 K. Calfumán, M. J. Aguirre, P. Cañete-Rosales, S. Bollo, R. Llusar and M. Isaacs, *Electrochim. Acta*, 2011, **56**, 8484.

57 M. M. -N. Zhang, Y. -T- Long and Z. Ding. *Chem. Cent. J*., 2012, **6**, 20.

58 J. Xu, W. Huang and R.L. McCreery, *J. Electroanal. Chem*., 1996, **410**, 235.

59 F. Kuang, D. Zhang, Y. Li, Y. Wan and B. Hou, *J. Solid State Electrochem.*, 2009, **13**, 385.

60 U. Hasse and F. Scholz, *Electrochem. Commun*., 2001, **3**, 429.

61 U. Hasse, J. Nieven and F. Scholz, *J. Electroanal. Chem*., 2013, **556**, 13.

62 U. Hasse, K. Wagner and F. Scholz, *J. Solid State Electrochem*., 2004, **8**, 842.

63 T. Grygar, *J. Solid State Electrochem*., 1998, **2**, 127.

64 T. Grygar, P. Bezdicka, D. Hradil, A. Doménech-Carbó, F. Marken, L. Pikna and G. Cepria, *Analyst*, 2002, **127**, 1100.

65 T. Grygar, J. Hradilova, D. Hradil, P. Bezdicka and S. Bakardjieva, *Anal. Bioanal. Chem*., 2003, **375**, 1154.

66 A. Doménech-Carbó, M. T. Doménech-Carbó, M. C. Saurí-Peris, J. V. Gimeno-Adelantado and F. Bosch-Reig, *Anal. Bioanal. Chem*. 2003, **375**, 1169.

67 T. Grygar, S. Kuckova, D. Hradil and D. Hradilova, *J Solid State Electrochem*. 2003, **7**, 706.

68 A. Doménech-Carbó, M. T. Doménech-Carbó and M. C. Saurí-Peris, *Talanta*, 2005, **66**, 769.

69 A. Doménech-Carbó, M. T. Doménech-Carbó, M. Calisti and V. Maiolo, *Talanta*, 2010, **81**, 404.

70 A. Doménech-Carbó, M. T. Doménech-Carbó, M. Calisti and V. Maiolo, *J. Solid State Electrochem*., 2010, **14**, 465.

Figures

Figure 1. Arrangements for SECM imaging of pictorial samples: a) parallel; b) transversal.

Figure 2. SECM topographic images of two microparticulate deposits of Naples yellow (K43100, *Kremer pigmente*) on Pt substrate immersed into 2.0 mM $K_4Fe(CN)_6$ plus 0.25 M HAc/NaAc, pH 4.75. a) E_T = +0.30 V; E_S = 0.00 V; b) E_T = +0.30 V; E_S = –0.30 V; c) E_T = +0.30 V; E_S = 0.00 V; d) E_T = +0.30 V; E_S = –0.70 V. Continuous (dotted) arrows mark regions where there is increase (decrease) of negative feedback features presumably associated to Pb deposition; dotted arrows mark the regions where there is topographic failure, due to the consumption of the parent pigment.

Figure 3. Probe approach curves of a microparticulate deposit of Naples yellow (K43100, *Kremer pigmen*te) on Pt substrate immersed into 2.0 mM $K_4Fe(CN)_6$ plus 0.25 M HAc/NaAc, pH 4.75. a) E_T = +0.30 V; E_S = 0.00 V; b) E_T = +0.30 V; E_S = –0.70 V.

Figure 4. SECM topographic images of a microparticulate deposit of Spanish ochre (K11585 *Kremer pigmente*) on Pt substrate immersed into 2.0 mM $K_4Fe(CN)_6$ plus 0.25 M HAc/NaAc, pH 4.75. a) E_T = +0.30 V; E_S = 0.00 V; b) E_T = +0.30 V; E_S = –0.45 V.

Figure 5. a,b) Topographic AFM image and c,d) amplitude error channel graphs of a deposit of hematite (K48651 *Kremer pigmente*) on a graphite plate in contact with 0.25 M sodium acetate buffer, pH 4,75, a,c) before, and b,d) after application of 10 potential cycles between 0.0 and -0.75 V at a sweep rate of 10 mV/s.

Figure 6. a,b) Amplitude error channel graphs and c,d) topographic images of a deposit of morin (Sigma-Aldrich) crystals attached to a graphite plate in contact with 0.25 M sodium acetate buffer, pH 4,75, a,c) before, and b,d) after application of an oxidative potential step at +0.45 V during 5 min.

Figure 7. Study of sample S1 from "*Los Jurados de Valencia ante la Inmaculada*" by Jerónimo Jacinto de Espinosa. a) SECM imaging upon placing the sample on the

substrate electrode in transversal position immersed into 2.0 mM $K_4Fe(CN)_6$ plus 0.25 M HAc/NaAc, pH 4.75. a) E_T = +0.30 V; E_S = 0.00 V. b) Microphotograph (PPL) of the paint strata of sample S1 corresponding to the cross-section in (a).

Figure 8. SECM topographic images of paint sample S2 arranged transversally on Pt substrate immersed into 2.0 mM $K_4Fe(CN)_6$ plus 0.25 M HAc/NaAc, pH 4.75. a) E_T = +0.30 V; E_S = 0.00 V; b) E_T = +0.30 V; E_S = –0.45 V; c) E_T = +0.30 V; E_S = –0.70 V.

Figure 9. SECM topographic images of paint sample S2 arranged transversally on Pt substrate immersed into 2.0 mM $K_4Fe(CN)_6$ plus 0.25 M HAc/NaAc, pH 4.75. a) E_T = +0.30 V; E_S = 0.00 V; b) E_T = +0.30 V; E_S = –0.70 V.

Figure 10. SECM topographic images of paint sample S3 arranged transversally on Pt substrate immersed into air-saturated 0.25 M HAc/NaAc, pH 4.75. Successive scanning experiments at E_T = –0.45 V and applying E_S values of: a) 0.00; b) +0.40; c) –0.20; d) –0.60 V. al: alizarin; az: azurite; lw: lead white.

Figure 11. SWV at the tip working electrode placed in the vicinity of paint sample S3 arranged transversally on Pt substrate immersed into air-saturated 0.25 M HAc/NaAc, pH 4.75 after the successive SECM experiments depicted in Figure 9 at E_S values of: a) +0.40; b) –0.20; c) –0.60 V. Potential scan initiated at a) +0.05 V; b) –0.65 V; c) –0.85 V in the positive direction. Potential step increment 4 mV; square wave amplitude 25 mV; frequency 5 Hz.

Figure 1.

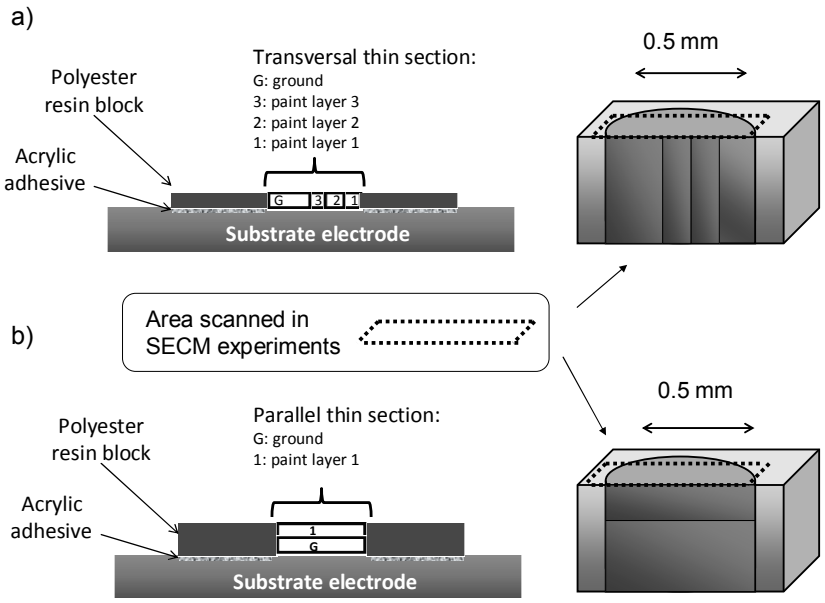

Figure 2.

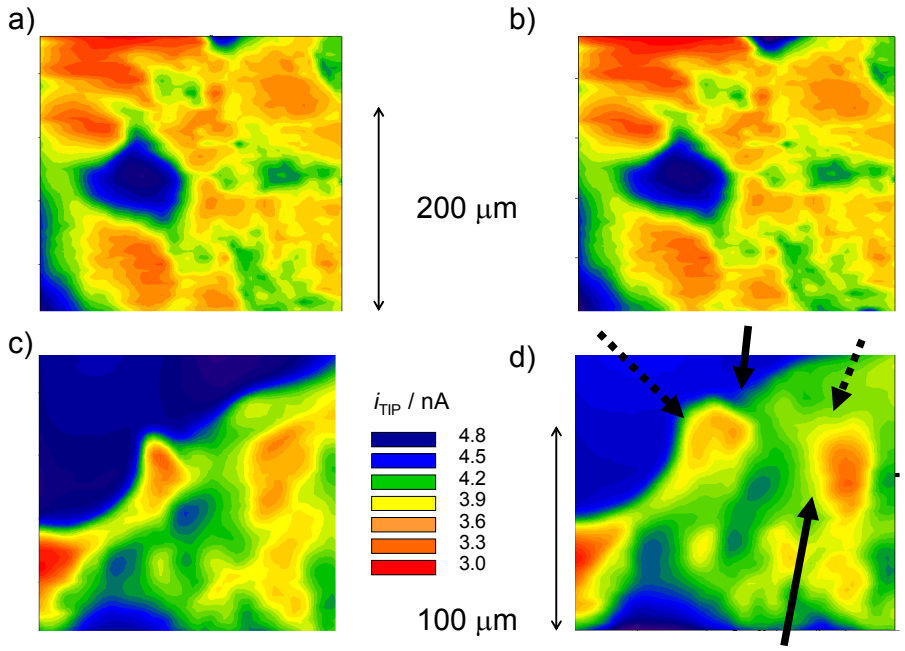

Figure 3.

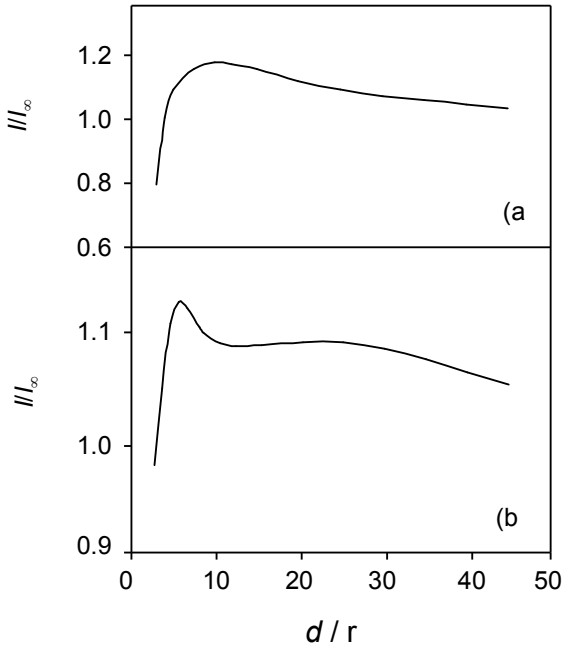

Figure 4.

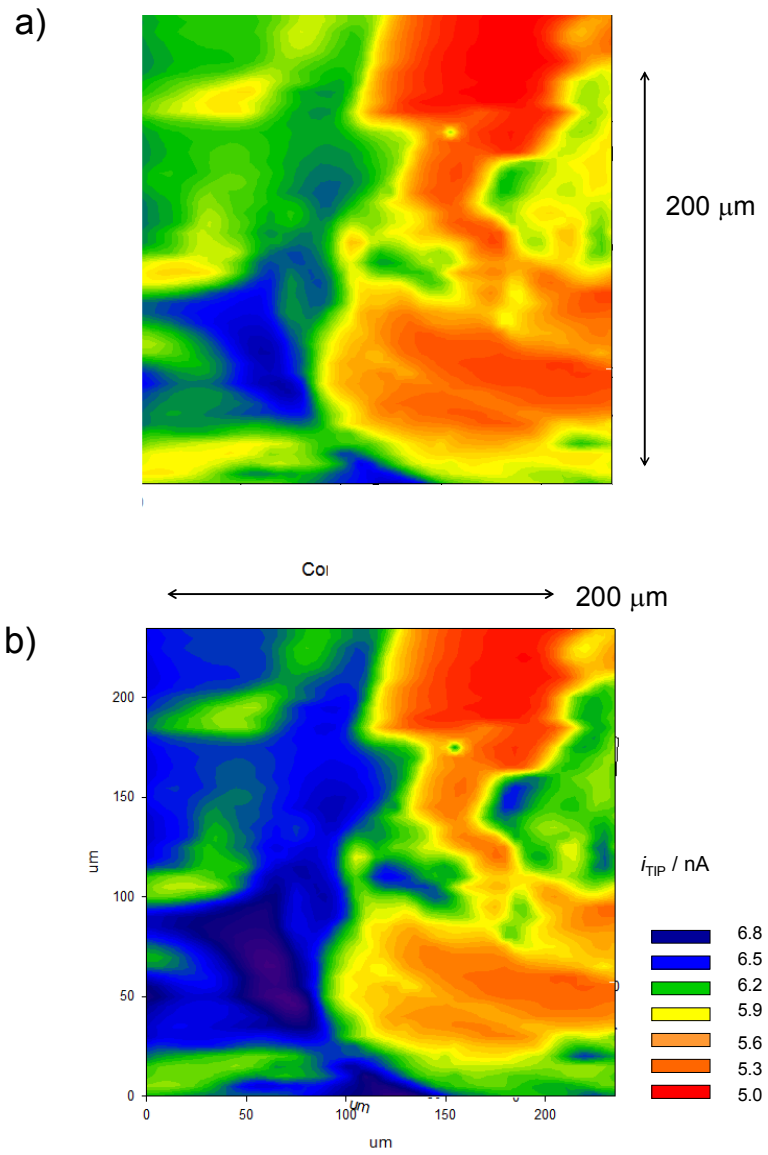

Figure 5.

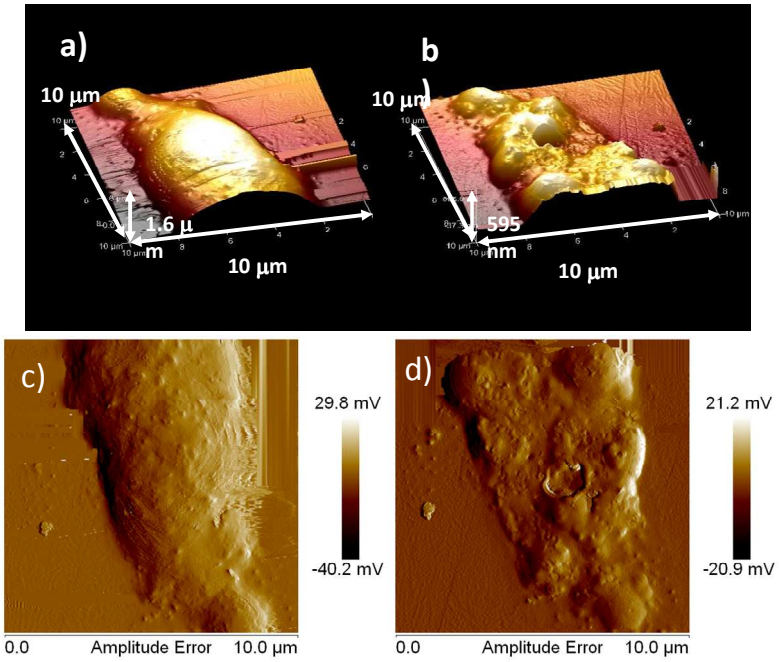

Figure 6.

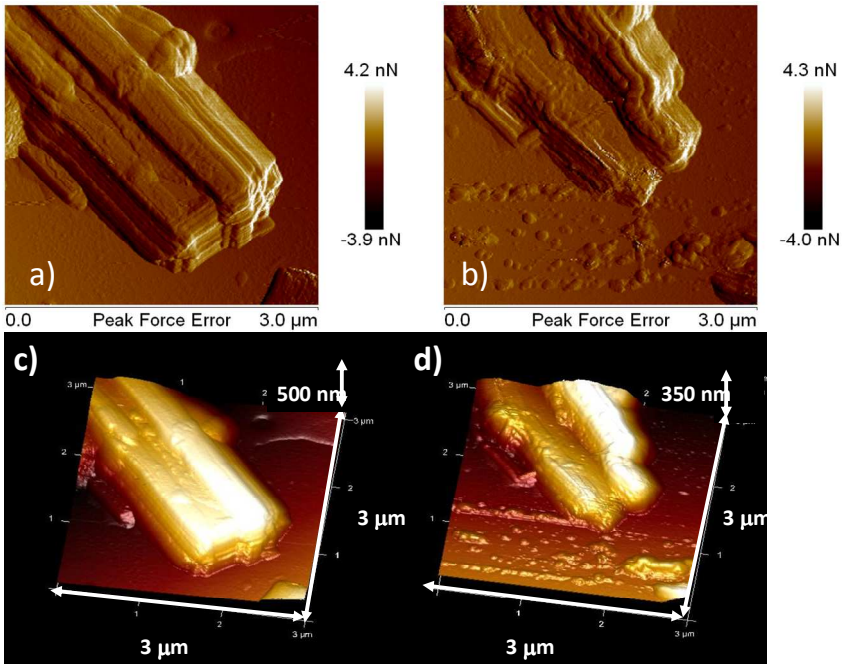

Figure 7.

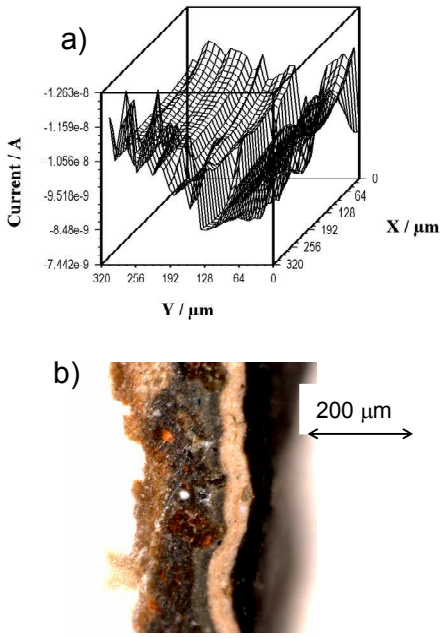

Figure 8.

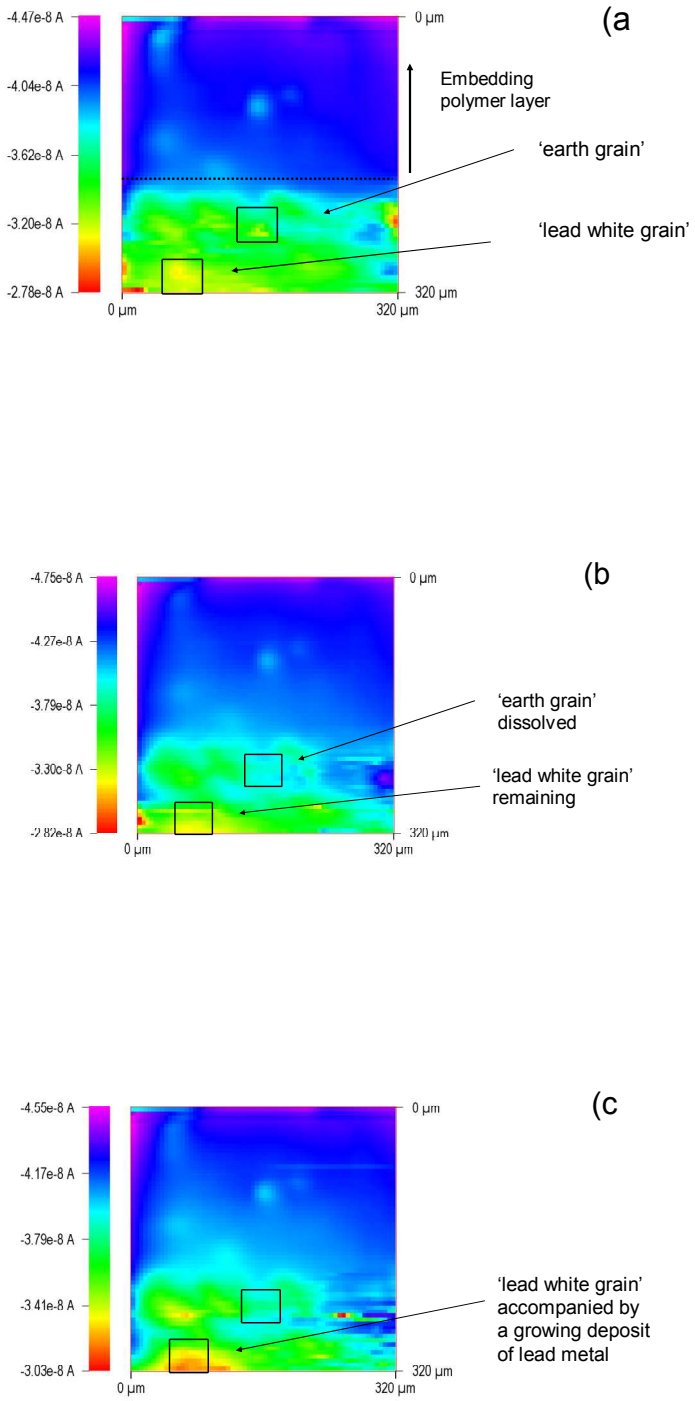

Figure 9.

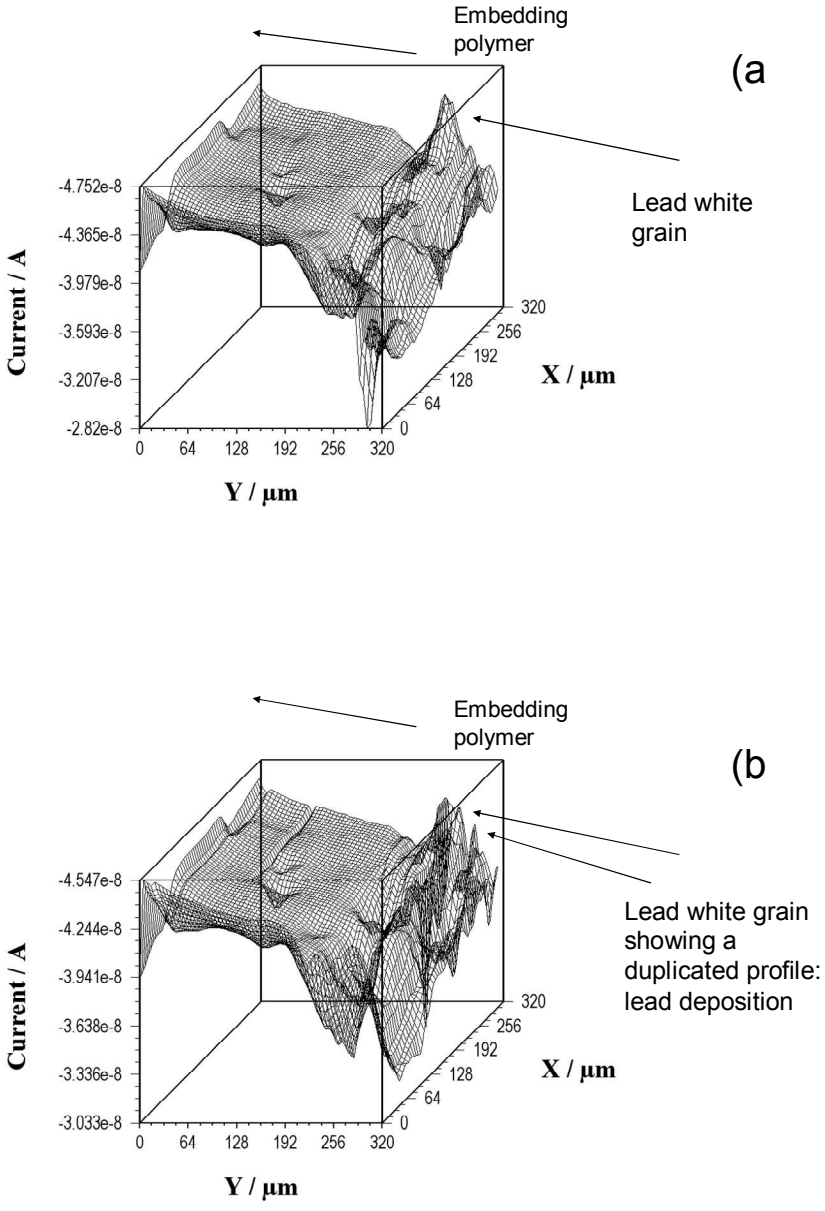

Figure 10.

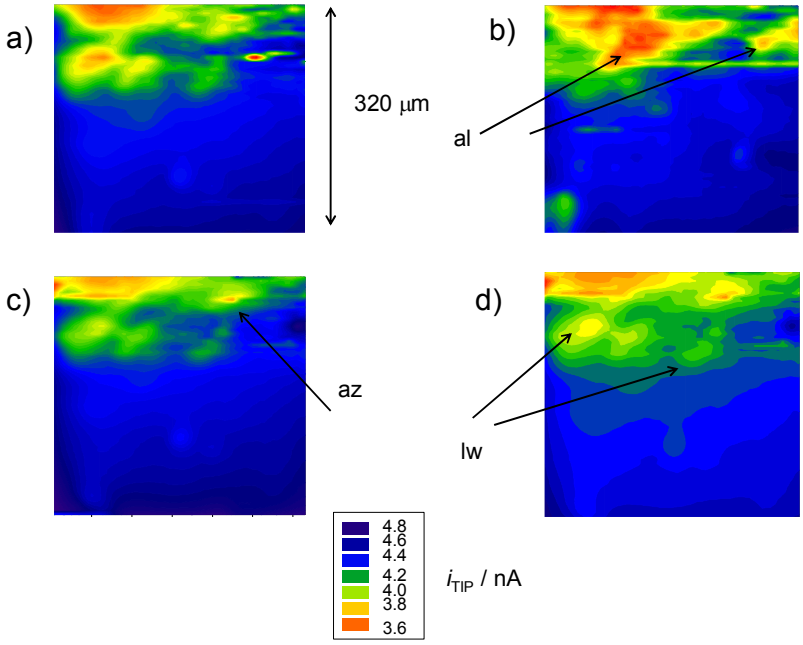

Figure 11.